

Insight into the electrical properties and chain conformation of spherical polyelectrolyte brushes by dielectric spectroscopy

Xiaoxia Guo and Kongshuang Zhao

College of Chemistry, Beijing Normal University, Beijing 100875, People's Republic of China

E-mail: zhaoks@bnu.edu.cn

Received 19 June 2016, revised 21 October 2016

Accepted for publication 27 October 2016


Published 12 December 2016



Abstract

We report here a dielectric study on three kinds of anionic spherical polyelectrolyte brush (SPBs, consisting of a polystyrene (PS) core and three different poly (acrylic acid) chains grafted onto the core) suspensions over a frequency ranging from 40 Hz to 110 MHz. The relaxation behavior of the SPB suspensions shows significant changes in the brush-layer properties when the mass fraction of SPBs and the pH of the suspensions change. Two definite relaxations related to the interfacial polarization are observed around 100 kHz and 10 MHz. A single-layer spherical-shell model is applied to describe the SPB suspensions wherein the suspended SPB is modeled as a spherical-shell composite particle in which an insulated PS sphere is surrounded by a conducting ion-permeable shell (the polyelectrolyte chain layer). We developed the curve-fitting procedure to analyze the dielectric spectrum in order to obtain the dielectric properties of the components of the SPBs, especially the properties of the polyelectrolyte brush. Based on this method and model, the permittivity and conductivity of the brush layer, ζ potential, etc are calculated. The ordered orientation of the water molecules in the layer leads to an additional electrical dipole moment; increasing pH causes the brush layer to swell. In addition, the repulsive force between the SPB particles are evaluated using the brush-layer thickness, which is obtained by fitting dielectric spectra, combined with relative theoretical formulas. Increasing PH values or SPB concentration would improve the stability of the SPBs dispersion.

Keywords: spherical polyelectrolyte brushes, electrical properties, chain conformation, dielectric spectroscopy

 Online supplementary data available from stacks.iop.org/JPhysCM/29/055102/mmedia

(Some figures may appear in colour only in the online journal)

1. Introduction

In the last two decades, spherical polyelectrolyte brushes (SPBs), which consist of a hard core with polyelectrolyte chains grafted onto it, have received tremendous attention because of their potential application in some fascinating fields [1–3]. According to the types of grafted polyelectrolyte chains, they could be divided into two classes of SPBs:

quenched and annealed [4]. The polyelectrolyte chain of a quenched SPB is independent of the pH, while the annealed brush is responsive to pH. Normally it is achieved by attaching weak polyelectrolytes as poly (acrylic acid) (PAA) to the surface of polystyrene (PS). Because the amount of charging on the chains depends on pH, pH plays a key role in determining the chemical natures and conformation of annealed brushes. Moreover, the ionic strength of both quenched and annealed

SPB suspension affects the interaction between charged segments. Hence, smart SPBs with different stimuli response to the environment have been developed and widely used in protein separation, catalysis, drug delivery and other fields [2, 3, 5, 6]. Ballauff *et al* reported that SPBs can achieve the adsorption and separation of protein by controlling the solution conditions, and they are deemed to be a new class of colloidal carrier particles [5]. In order to improve the catalytic activity of nanoparticles, PS-PAA SPBs were used to synthesize Ag nanoparticles *in situ* by UV irradiation [6], and just recently, an interesting application of SPBs was reported by the same group, which was that the catalytic activity of Au/Pd nanoalloys immobilized in SPBs is strongly enhanced [3].

On the other hand, studies on the fundamental nature of SPBs have been reported [4, 7, 8]. SPBs create a model of a soft particle in which a hard particle core and bulk solution are separated by a polyelectrolyte chain layer. Such SPB suspension can be used as a model system to study colloidal stability. It is well known that the electrostatic repulsion between two charged particles can stabilize a colloid solution. Moreover, the space location-obstruct effect prevents the particles from approaching each other, and the two factors stabilize the colloidal suspension. Because the charged polyelectrolyte chains can prevent the condensation of particles, both the electrostatic and steric repulsion effects of SPBs contribute to the stability of a colloidal system [9]. Considering that special constitutions of SPBs and their adjustable brush layers (or soft layers) are made up of polyelectrolyte chains, the importance of SPBs is not only limited to colloid and interface science, but also stretches to many other fields, such as controlled synthesis and self-assembly in chemistry, materials and life science [2]. Hence, a comprehensive understanding of the essential properties of the brush layer of SPBs would be extremely beneficial. Fundamental studies of SPBs have been performed in recent years [10, 11]. Pincus studied the stability of colloid particles with grafted polyelectrolyte chains, and indicated that the stability can be controlled by changing the charge character of polyelectrolyte chains [9]. Subsequently, the studies mainly focused on the charge distribution in the brush layer [12], the effects of pH, ionic strength and valency of counterions on the chain configuration [4, 7]. Additionally, zeta potential has also been used to assess the strength of the repulsive force and thus the stability of the SPB dispersion [13].

Actually, although all studies on SPBs agreed on the existence of the potential distribution in the brush layer and the effect of ion concentration on the zeta potential, several questions remain unclear. The most important of which is that the long polyelectrolyte chains grafted onto the particle surface complicate the surface potential measurements. A reliable potential value is difficult to deduce considering the complicated morphology of the chain layer controlled by valence, concentration, and the distribution of counterions around the fixed charge on the chains [11]. To solve this problem, Dukhin and Zimmermann developed an approach to deduce the electrical parameter of the brush layer [14], as well as the structure, by measuring the surface conductivity [15, 16]. They found that pH and ionic strength in the brush layer strongly influence the values of zeta potential because of the

conformation transition of the brush layer. Also, the surface conductivity at the grafted polyelectrolyte brush layer can be estimated using the mobility of counterions. The conformation of the polyelectrolyte chains, the charge distribution within the polyelectrolyte layer and the migration of the counterions in the brush layer will impact on the stability of SPB suspensions.

So far, various experimental methods have been adopted to characterize the SPBs, especially the brush layer. Enormous information about the electrical properties and conformational transformation inside the layer as the medium environment changes has been obtained. For example, dynamic light scattering (DLS) can directly obtain the overall dimensions of SPBs [7], cryogenic transmission electron microscopy collects images of SPBs with a well-outlined brush layer [8]. Dielectric relaxation spectroscopy (DRS) has been extensively applied to study the dynamic and structural properties of materials [17, 18]. In recent years, increasing interest has been attracted to the study of the dielectric properties of colloidal particles [19–22]. By analyzing DRS, valuable electrical and structural information about colloidal particles can be obtained with appropriate electrical models. Delgado *et al* studied the dielectric properties of SPB suspensions and found an enormous loss peak related to the dynamic mobility in the kHz frequency range [21]. In addition, they expounded that the huge dielectric increment was caused by the inhomogeneity of the counterion distribution in the brush layer [22]. Recently, Cametti *et al* studied the dielectric properties of several types of soft-particle suspension including ionic thiol-coated and PLGA-based nanoparticle suspensions. Valuable information about the electrical properties at the interface was obtained [23, 24].

Another advantage of studying SPBs is the well-defined core-shell structure, which is an exact model for soft particles. Except SPBs, soft particles cover many natural and synthetic systems, i.e. colloidal particles onto which block polymer, surfactant and biodegradable or biocompatible material are grafted or absorbed [25]. Therefore, fundamental research of soft particles has attracted much attention. Ohshima derived a general expression for conductivity of concentrated soft particles and revealed the potential distribution in the soft layer [26]. Moreover, he correlates the ionic strength, conductivity, and ionic strength with the Donnan potential, which is the surface potential of a spherical soft particle in the electrolyte solution [27, 28]. All of these colloidal features are highly related to the dielectric properties of the soft layer [26, 29].

Whether the dielectric theories and models for hard particles are suitable for the present soft-particle system is of major interest. It is well known that the dielectric theory of typical particle dispersion, developed nearly half a century ago, has been successfully applied in many practical systems [19, 20]. At present, well-developed dielectric theories and models can give a good explanation for the relaxation behaviors of most particle suspensions. In particular, their relaxation mechanisms have been attributed to surface diffusion [30] and volume diffusion for lower frequency [31] and interfacial polarization for higher frequency [32], respectively. However, although some soft-particle systems have been studied by dielectric spectroscopy, detailed analysis of the relaxations remains insufficient

for two reasons: dielectric behaviors of two relaxations are hard to observe experimentally; there are many uncertain factors to analyze in dielectric data of low frequency (LF) because of the introduction of polyelectrolyte chains onto hard particles. A key problem the detection of the relaxation caused by the polyelectrolyte brush. Fortunately, Delgado provided us with an instructive example: a low-frequency relaxation related to the polyelectrolyte brush layer [21].

Cametti elaborated how the structure of polymer soft layer alters the dielectric response and the electrokinetic properties of the system, as well as the electrokinetic properties of the soft layer, with the possibility of theoretical analysis pointed out in his review [33]. The soft layer, which is ion-permeable and distributive, like SPBs, can also be described by theoretical models. As far as we know, however, studies into the theoretical analysis of the observed dielectric data is inadequate, because current dielectric studies are not comprehensive. Detailed information on the electrical and structural properties of the constituent phases of SPBs (e.g. the permittivities and conductivities of the brush layer and polymer core, and the thickness of the brush layer) cannot be estimated. In our previous research, dielectric spectra with two relaxation processes observed in the PS-PAA SPB suspension were successfully analyzed by using Hanai equation and a typical model for hard-particle suspension [34]. The SPB is regarded as a particle dispersed in a continuous medium. However, the study did not elucidate the electrical properties of each constituent in the SPBs, i.e. the PS hard core and PAA polyelectrolyte chain layer. Moreover, the analysis failed to taking into account information about the varying soft-layer boundary in different medium environments due to the limited analysis model. In other words, the indistinct boundary of soft particles proposed by Cametti and Grosse has not been solved yet [33, 35].

As early as 1946, the spherical-shell model was proposed and proved as a valid model to describe conventional colloidal particle dispersion or biological cell suspension. Hanai–Asami *et al* have already established a quantitative analytical calculation method [36, 37]. However, such a model and corresponding computing approach are based on the object of a spherical-shell particle in which the shell is impermeable and non-conductive. Therefore, it is inappropriate for the SPB suspension. Dukhin and Shilove [38] proposed a model including the diffusion and exchange of ions between the electrical double layer and the bulk phase. Afterward, Grosse and Zimmerman [39] extended the Dukhin–Shilove model to a new one in which the sphere core is covered with a charged single shell, and presented a calculation method to obtain the analytical solution. Recently, Asami [40] successfully examined the dielectric dispersion of *Escherichia coli* cell suspensions by using the Gross–Zimmerman (G–Z) model.

In this work, the dielectric spectra of SPBs with an annealed brush is studied. The SPBs consisting of a nanoscale PS core and PAA chains of three kinds of different length are modeled as a PS core covered with an ion-permeable PAA layer. The dielectric data are recorded as a function of the mass fraction of SPBs and pH as well as chain length. Two relaxation processes observed around 100 kHz and 10 MHz, respectively, are

analyzed based on the proposed model. For the analysis, we derive the theoretical formulas from the Gross–Zimmerman model, and deduce the electrical parameters of the PS core and PAA brush layer under different medium environments. With these parameters, the diffusion migration of counterions in the brush layer, conformation of PAA chains as the mass fraction of SPBs and pH of bulk solution changing is investigated. The dielectric behavior of SPBs of different PAA chain lengths and their corresponding electrical parameters are compared quantitatively.

2. Dielectric model of SPBs and relevant formulas

SPBs consist of polyelectrolyte chains densely grafted onto the surface of microspheres to constitute a special soft particle and have two basic features: the brush layer is charged and ion-permeable. Thus, SPB suspension contains three ‘phases’ of different electrical properties: polymer core, brush layer grafted onto the polymer, and medium solution. According to Maxwell–Wagner interfacial polarization theory, for such three-phase SPB suspensions two relaxations exist under the external AC electric field [41]. The electrical parameters of the three phases can be calculated by analyzing the two relaxations using the spherical-shell model, that is, a sphere covered with a shell of uniform electrical conductivity. However, this method is inappropriate for SPB suspension because of its special shell. Dukhin and Shilove [38] proposed a model to illuminate the diffusion and exchange of ions between the electrical double layer and the bulk phase. Following this, many modified models have been reported [20, 39]. Among these models, a soft-sphere model was developed along the lines of the Dukhin–Shilove model by Grosse and Zimmerman in 2005 [39] and is widely used. This model is similar to the traditional spherical-shell mode. Moreover, the surface conductivity on the soft layer was considered, as well as the features of this layer, i.e. that it is charged and ion-permeable. Additionally, the analysis formulas for the calculation of the electrical parameters of soft layer were derived. Therefore, the Gross–Zimmerman model is suitable for analyzing the present SPB suspensions.

In the present work, SPB suspension is modeled and depicted in figure 1(b). The suspended SPB particle with complex permittivity ϵ_p^* is modeled as an insulating PS sphere with radius a and complex permittivity ϵ_i^* , which is surrounded by a conducting ion-permeable shell (polyelectrolyte chain layer) with thickness d_s and complex permittivity ϵ_s^* , as schematically depicted in figure 1(b). Such SPB particles are dispersed in a salt-free continuous medium of complex permittivity ϵ_a^* with volume fraction Φ and constitute SPB suspension (see figure 1(a)). The mobile counterions in SPB suspensions are mainly caused by the dissociation of the carboxyl group on PAA chains in the shell layer (see figure 1(c)) and bulk phase. And the ions can penetrate into the soft-shell layer, i.e. the exchange of ions between the shell layer and bulk phase can occur at the interface $R_s = (a + d_s)$. This consideration is different from the conventional models, such as Hanai–Asami, previously adopted to describe microcapsules and biological cells.

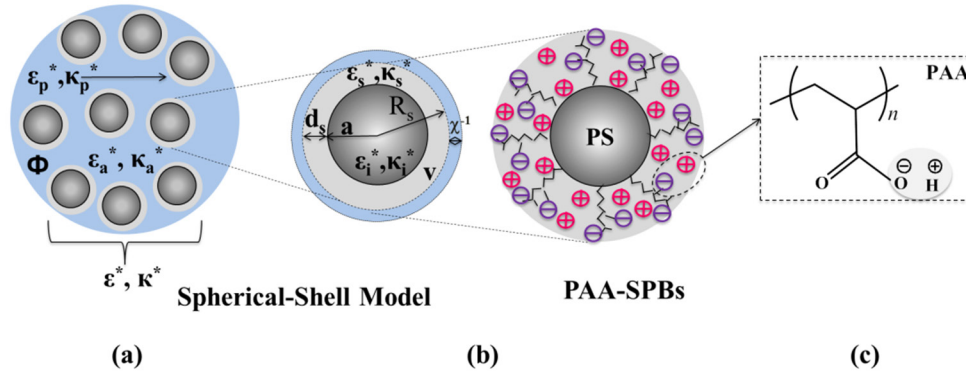


Figure 1. Dielectric (spherical-shell) model of SPB suspension ((a)–(b)), where a is the radius of sphere, d_s is the shell thickness and R_s is equal to the sum of a and d_s . The structure of anionic PAA polyelectrolyte chains (c).

We assume that: (a) the mass distribution of the polyelectrolyte chains in the shell phase is uniform and (b) the fixed charges of SPB particles are also uniformly distributed in the shell and that the permittivity of the shell should be equal everywhere.

Based on the above model, the complex permittivity of the SPB suspension ε^* is described by the following Wagner equation as

$$\varepsilon^* = \varepsilon_a^* \left(1 + \frac{3\phi d^*}{1 - \phi d^*} \right). \quad (1)$$

When the SPBs' mass fraction is very low, e.g. $\Phi \ll 1$ (the present work follows this condition), equation (1) is simplified to

$$\varepsilon^* = \varepsilon_a^* (1 + 3\phi d^*) \quad (2)$$

where $\varepsilon_a^* = \varepsilon_a + \kappa_a/(j\omega\varepsilon_0)$ (ε_a and κ_a are the permittivity and conductivity of the medium respectively, $\omega = 2\pi f$ is angular frequency (f is measuring frequency), $j^2 = -1$ and ε_0 are the permittivity of the vacuum); d^* is the dipole coefficient (or Clausius–Mossotti function) which is used to calculate effective dipole moment. The coefficient d^* depends on both the dielectric properties of the particle and medium and the frequency of the applied field, and d^* can be expressed as the sum of the dipole coefficients at low and high frequency (HF) [39, 40, 42]:

$$d^*(\omega) = d_\infty - \frac{\Delta d_L}{j\omega\tau_L + 1} - \frac{\Delta d_H}{j\omega\tau_H + 1} = d_H^* + d_L^*. \quad (3)$$

The dipole coefficients of LF d_L^* originate from the polarization due to the diffusion and permeation of the counterion in the soft layer [43], and can be written as

$$d_L^* = \Delta d_L \frac{1 + \sqrt{2/S} \sqrt{j2\pi f \tau_L}}{1 + \sqrt{2/S} \sqrt{j2\pi f \tau_L} + j2\pi f \tau_L} + d_{Lh}, \quad (4)$$

where $\Delta d_L = -6S \left(\frac{R^+ - R^-}{R^+ + R^- + 4} \right)^2$, $\tau_L = \frac{SR_s^2}{2D}$, S , and d_{Lh} are given in the appendix. The dipole coefficient of HF d_H^* is related to interfacial polarization between the particles and the medium and is given by

$$d_H^* = \frac{\varepsilon_p^* - \varepsilon_a^*}{\varepsilon_p^* + 2\varepsilon_a^*} \quad (5)$$

where the complex permittivity ε_p^* of the dispersed particles is given by

$$\varepsilon_p^* = \frac{1}{j2\pi f \varepsilon_0} \frac{2\lambda}{R_s} + \varepsilon_s^* \frac{\varepsilon_i^* + 2\varepsilon_s^* + 2v(\varepsilon_i^* - \varepsilon_s^*)}{\varepsilon_i^* + 2\varepsilon_s^* - v(\varepsilon_i^* - \varepsilon_s^*)} = \varepsilon_p - j\varepsilon_p'', \quad (6)$$

wherein $v = [1 - d_s/(a + d_s)]^3$, which represents the volume fraction of the PS sphere in the whole SPB particle. According to Hanai's method [44], the complex permittivity ε_i^* of the PS spheres and ε_s^* of the polyelectrolyte brush layer are expressed by the relaxation parameters (ε_m and ε_h are the limit of permittivity at the middle and high frequencies respectively, κ_l denotes LF limits of conductivity, and f_0 is the characteristic relaxation frequency) measured experimentally as:

$$\varepsilon_s^* \frac{\varepsilon_i^* + 2\varepsilon_s^* + 2v(\varepsilon_i^* - \varepsilon_s^*)}{\varepsilon_i^* + 2\varepsilon_s^* - v(\varepsilon_i^* - \varepsilon_s^*)} = \varepsilon_h + \frac{\varepsilon_m - \varepsilon_h}{1 + (f/f_0)} + \frac{\kappa_l}{j\omega\varepsilon_0}. \quad (7)$$

Here, ε_i^* and ε_s^* are defined with their permittivity ε_i , ε_s and conductivity κ_i , κ_s as $\varepsilon_i^* = \varepsilon_i + \kappa_i/(j\omega\varepsilon_0)$ and $\varepsilon_s^* = \varepsilon_s + \kappa_s/(j\omega\varepsilon_0)$ (see figure 1).

There relaxation parameters are respectively expressed by phase parameters of SPB particles as follows:

$$\varepsilon_h = \varepsilon_s \frac{\varepsilon_i + 2\varepsilon_s - 2v(\varepsilon_s - \varepsilon_i)}{\varepsilon_i + 2\varepsilon_s + v(\varepsilon_s - \varepsilon_i)} \quad (8)$$

$$\Delta\varepsilon = \varepsilon_l - \varepsilon_h = \frac{9v(1-v)(\varepsilon_s\kappa_i - \varepsilon_i\kappa_s)^2}{[2\varepsilon_s + \varepsilon_i + v(\varepsilon_s - \varepsilon_i)] + [2\kappa_s + \kappa_i + v(\kappa_s - \kappa_i)]^2} \quad (9)$$

$$f_0 = \frac{2\kappa_s + \kappa_i + v(\kappa_s - \kappa_i)}{2\pi\varepsilon_0 [2\varepsilon_s + \varepsilon_i + v(\varepsilon_s - \varepsilon_i)]} \quad (10)$$

$$\kappa_l = \kappa_s \frac{2\kappa_s + \kappa_i - 2v(\kappa_s - \kappa_i)}{2\kappa_s + \kappa_i + v(\kappa_s - \kappa_i)}. \quad (11)$$

The surface-charged state of SPB particles depends on spatial distribution of ions, and the surface-charge density σ_0 of SPBs determines the zeta potential ζ of the SPB particles:

$$\sigma_0 = \sqrt{8RT\varepsilon_a\varepsilon_0c_a} \sinh(F\zeta/2RT) \quad (12)$$

where c_a is the concentration of the continuous medium in mM, F is the Faraday constant, R is the gas constant and T is the absolute temperature.

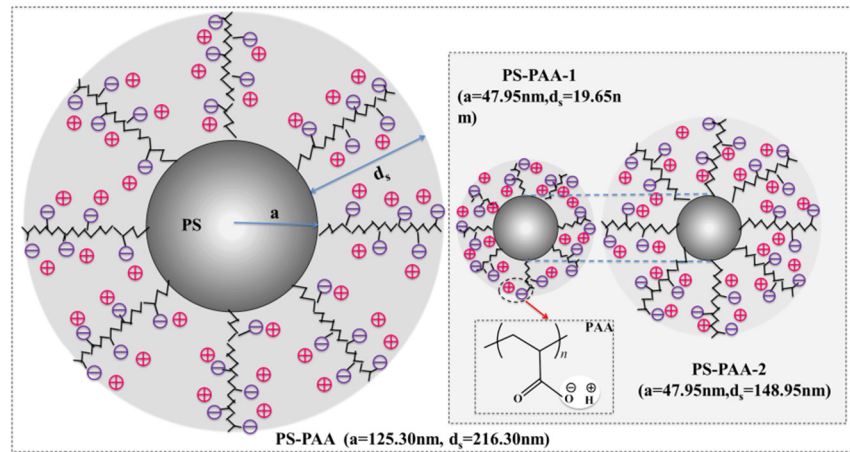


Figure 2. Sketch of three kinds of SPBs investigated. Linear chains of poly(acrylic acid) are chemically grafted onto the surface of a colloidal poly(styrene) particle. The radius a of the core particles and the radius of SPBs R_s ($=a + d_s$) are measured by DLS (see table 1). \oplus , H^+ ; \ominus , $-COO^-$.

According to the interfacial polarization theory induced by surface conductance λ [45], σ_0 is proportional to the relaxation strength $\Delta\epsilon$. Hence, σ_0 is deduced by equation (8) with corresponding phase parameters and structure parameters given in figure 1. The phase parameters of various compositions of SPB particles are obtained by fitting equations (1)–(7) to the observed dielectric spectra. From d_L^* and d_H^* [39], the surface conductance λ is an important parameter in the Grosse–Zimmerman model. It can be expressed as

$$\lambda = \frac{R^+ + R^-}{4} R_s \kappa_a. \quad (13)$$

Here, the expressions of the intermediate variable R^+ and R^- are in the appendix.

3. Experimental section

3.1. Materials and preparation of sample

3.1.1. Materials. All the chemicals used for this experiment were of analytical grade. Styrene (Sigma-Aldrich) and acrylic acid (Sigma-Aldrich) are distilled under a reduced pressure to remove the inhibitor, and stored at 4 °C in a refrigerator. Sodium dodecyl sulfate (SDS) (Merck) is recrystallized before being used as a surfactant in the synthesis of polymer cores. Potassium persulfate (KPS) (Merck) is used without further purification. Doubly distilled water is used in this experiment.

3.1.2. Synthesis and characterization of anionic SPBs. The anionic SPBs used in this work are synthesized by photo-emulsion polymerization, which is based on a ‘grafting-from’ technique, leading to a dense layer of chemically bound polyelectrolyte chains. First, HMEM photoinitiator is prepared by a Schotten–Baumann reaction. Second, styrene is polymerized in a certain amount of H_2O using SDS as surfactant and KPS as initiator [1]. Then, HMEM is added under starved conditions. After adding polystyrene emulsion, acrylic acid and pure water to photoreactor under UV irradiation (wavelength range

Table 1. Some information about the three SPBs investigated.

SPBs	a/nm	d_s/nm	$R_s (=a + d_s)/nm$
PS-PAA	125.3	216.30	341.6
PS-PAA-1	47.95	19.65	67.6
PS-PAA-2	47.95	148.95	196.9

of 200–600 nm), HMEM photoinitiator rapidly produces free radicals to promote the growth of PAA brush. Finally, functional monomers are grafted onto the PS core surface [46]. The whole reaction is carried out under magnetic stirring and nitrogen protection. This specific preparation method has been reported elsewhere [47].

The radius of SPBs (R_s) and the PS core (a) are determined by DLS (a Peters ALV 4000 light scattering goniometer). The thickness d_s of SPBs is defined as the difference between R_s and a . A sketch of the schematic and structural information of three kinds of SPBs used in this study, which are PS-PAA, PS-PAA-1 and PS-PAA-2, is shown in figure 2 and table 1.

3.1.3. Preparation of samples. SPBs with a PS core and brush-like PAA shell are prepared by photo-emulsion polymerization as described above. Then, the SPBs solution is freeze-dried (LGJ-18S freezing dryer, Beijing Songyuan Huaxing Technology Develop Co. Ltd) and diluted to a certain mass fraction by adding determined amount of deionized water. For PS-PAA-1, PS-PAA-2 suspensions, the mass fraction ranges from 9 to 0.1%, while for PS-PAA suspensions, the mass fraction ranges from 1.5 to 0.1%; the pH between 3 and 11 is adjusted by adding a different concentration of HCl or KOH aqueous solution. The pH is monitored by a microprocessor pH meter (UltraBASIC-7, Denver Instrument, China). Normally ionic strength is 10^{-4} M after the system has been adjusted carefully by adding different concentrations of KCl solution. Then, the sample is conducted in ultrasonic for 3 h and static for 24 h before dielectric measurements.

3.2. Dielectric measurements

Dielectric measurements of the SPB suspensions were carried out using an HP4294A Precision Impedance Analyzer (Agilent Technologies) over a frequency range from 40 Hz to 110 MHz, controlled by a personal computer. The amplitude of the applied alternating field was 500 mV. The measuring cell used in the test for the case of SPB suspensions is a parallel plate capacitor of platinum discs coated with platinum black and separated by a Lucite spacer (see figure S1 (stacks.iop.org/JPhysCM/29/055102/mmedia)). The geometric area of the electrodes is 13.72 mm² and the distance between the electrodes is 9.82 mm). To eliminate the errors from residual inductance (L_r) and stray capacitance (C_r) (the values of L_r , C_r and cell constant C_1 have been determined by using several standard substances (air, ethanol, water) and KCl solution of different concentrations are 26.8 nF · S⁻², 0.337 pF and 0.034 pF, respectively), the raw experimental data, capacitance C_x and conductance G_x are corrected according to Schwan's method [48] from the following equations:

$$C_s = \frac{C_x(1 + \omega^2 L_r C_x) + L_r G_x^2}{(1 + \omega^2 L_r C_x)^2 + (\omega L_r G_x)^2} - C_r \quad (14)$$

$$G_s = \frac{G_x}{(1 + \omega^2 L_r C_x)^2 + (\omega L_r G_x)^2}. \quad (15)$$

The corrected capacitance C_s and conductance G_s are converted to the corresponding dielectric permittivity ε and conductivity κ through the equations $\varepsilon = C_s/C_1$ and $\kappa = G_s \varepsilon_0/C_1$. All dielectric measurements are performed at (298 ± 0.5 K).

3.3. Determination of relaxation parameters

The dielectric response of a substance or system to applied AC electric field can be characterized by the complex permittivity ε^* which is defined as:

$$\varepsilon^*(\omega) = \varepsilon(\omega) - j \frac{\kappa(\omega)}{\varepsilon_0 \omega} = \varepsilon(\omega) - j \left(\varepsilon''(\omega) + \frac{\kappa_1}{\omega \varepsilon_0} \right), \quad (16)$$

where $\varepsilon(\omega)$ and $\kappa(\omega)$ are the frequency-dependent real part of complex permittivity and complex conductivity, respectively, and $\varepsilon''(\omega)$ is the frequency-dependent dielectric loss. For aqueous solution systems with higher electrolyte contents, like our samples, a considerable electrode polarization (EP) generally occurs in a lower frequency range. The conductivity of the whole system contains two contributions, one from LF conductivity κ_1 which can be obtained through the $\kappa''-\kappa$ plot. The imaginary part κ'' of the conductivity can be calculated from the obtained dielectric parameters ε_h : $\kappa'' = \varepsilon_0 \omega (\varepsilon - \varepsilon_h)$, and the other from dielectric loss ε'' which is calculated from the conductivity spectra through the equation $\varepsilon''(\omega) = (\kappa(\omega) - \kappa_1)/\omega \varepsilon_0$. The following empirical function, namely a combination equation of the i Havriliak–Negami (HN) function and the EP term, including i (the number of relaxations, usually $i = 1, 2$ or 3) Cole–Cole's terms and an EP term $A\omega^{-m}$ (A and m are adjustable parameters) is employed to analyze the experimental spectra:

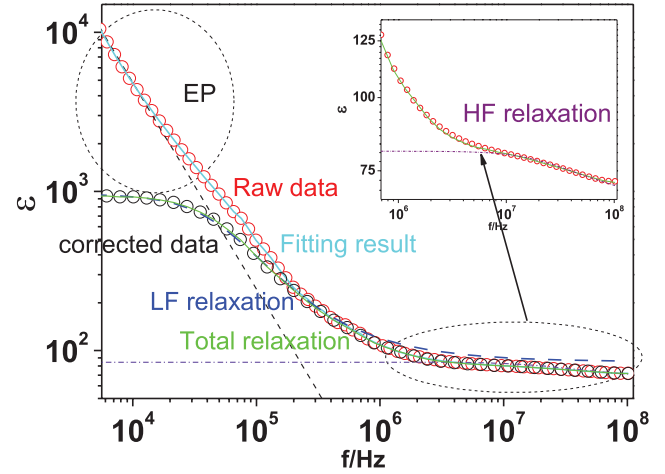


Figure 3. Frequency dependence of permittivity (hollow red circles) of pH 3.27 for wt_{PAA-SPB}% = 1.5%: solid cyan line, the best total fit with EP; hollow black circles, corrected data; solid green line, the best total fit for corrected data; short dashed black line, EP term; dashed blue line, LF relaxation; dashed dotted violet line, HF relaxation. The inset shows an expanded view of the HF dispersion with the best-fit curves.

$$\varepsilon^* = \varepsilon_h + \sum_i \frac{\Delta \varepsilon_i}{[1 + (jf/f_{0i})^{\alpha_i}]^{\beta_i}} + A\omega^{-m}. \quad (17)$$

Here, $\Delta \varepsilon_i$ is the relaxation intensity (i.e. relaxation increment) of relaxation i , f_{0i} is the characteristic relaxation frequency, and α and β are the distribution parameters of relaxation times ($0 < \alpha \leq 1$, $0 < \beta \leq 1$).

For systems with two dielectric relaxations (i.e. $i = 2$ in equation (17)), $\Delta \varepsilon_1 = \varepsilon_l - \varepsilon_m$ and $\Delta \varepsilon_2 = \varepsilon_m - \varepsilon_h$ (the subscripts 1 and 2 refer to the lower- and higher-frequency relaxation, and the l, m, and h are the low-, middle-, and HF limits of permittivity, respectively). The high- and middle-frequency limits of conductivity, κ_h and κ_m can be calculated using the following equations derived based on [49]:

$$\kappa_m = ((\varepsilon_l - \varepsilon_m)2\pi f_l \varepsilon_0) + \kappa_l \quad (18)$$

$$\kappa_h = ((\varepsilon_m - \varepsilon_h)2\pi f_h \varepsilon_0) + \kappa_m. \quad (19)$$

Figure 3 represents an example of the frequency dependence of permittivity (hollow red circles) of 1.5% PS-PAA SPB suspensions at pH = 3.27. It should be noted in figure 3 that the EP effect at the LF range (circled by a dashed ring) is well eliminated, and the corrected permittivity (hollow black circles) shows a clear-cut platform of the LF relaxation (the imaginary of complex conductivity also shows the EP in the LF and two relaxations occur around 100 kHz and 10 MHz, respectively: see figure S2(c)) [50]. We used the two HN and the EP terms (equation (17)) to fit the dielectric data; the cyan solid line is the fitting result in figure 3. After subtracting the EP term, we can display a measured spectra without the EP term (see the green solid line in figure 3). The values of $\Delta \varepsilon_1$, $\Delta \varepsilon_2$, f_{01} , f_{02} , and α_1 , α_2 , β_1 , β_2 , i.e. the relaxation parameters in equation (17), are determined by the non-linear least squares method to minimize the residual χ^2

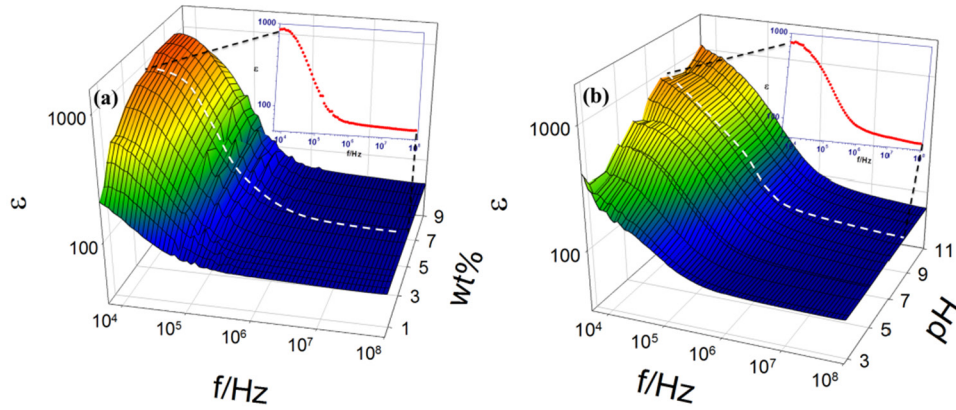


Figure 4. 3D representations of mass-fraction dependence of the real part of complex permittivity spectra of (a) and pH dependence of the real part of complex permittivity spectra when the mass fraction of SPBs is 0.3% (b) for the PS-PAA-2 suspension. They have been processed by eliminating the electrode polarization. The inset shows the real part of complex permittivity spectra at $w_{\text{SPB}} = 7.0\%$ and $\text{pH} = 9$, respectively.

$$\chi^2 = \sum_i \left\{ \log \text{Re}[\varepsilon_{\text{obs}}^*(f_i)] - \log \text{Re}[\varepsilon_{\text{the}}^*(f_i)] \right\}^2, \quad (20)$$

where $\text{Re}[\varepsilon_{\text{obs}}^*(f_i)]$ and $\text{Re}[\varepsilon_{\text{the}}^*(f_i)]$ are the real parts of the observed and theoretical complex permittivities, respectively. f_i is the i th measuring frequency. There are other effective methods to eliminate for fitting dielectric data, such as the HN expression with DC conductivity. This method is very effective for substantial materials and is described in the literature [51, 52].

It is clear from the fitting result that two sub-relaxation processes, namely the LF and HF relaxation (inset of figure 3 gives its expanded view), respectively, contribute the dielectric spectroscopy. Here, LF and HF relaxations correspond to $\Delta\varepsilon_1$ and $\Delta\varepsilon_2$, respectively. They are both essentially connected with interfacial polarization based on the foregoing model shown in figure 1. In addition, the LF relaxation of $f_{01} \approx 2 \times 10^5$ Hz is clearly separated from the HF dispersion around 30 MHz.

4. Results and discussion

4.1. Dielectric spectra of SPB suspensions of varying SPB mass fraction and pH

Figures 4(a) and (b) show the 3D representations for mass fractions of SPB dependence and pH dependence of the dielectric spectra, respectively. Note that figure 4 is the dielectric spectra after eliminating the EP effect. All of these dielectric spectra data were represented by equation (17) with the best-fit relaxation parameters ($\Delta\varepsilon_1$, $\Delta\varepsilon_2$, f_{01} , f_{02} , α_1 , α_2 , β_1 , β_2). Obtained main parameters, such as the low-, middle-, and high-frequency limits of permittivity ε_l , ε_m , ε_h and their characteristic frequency f_{01} , f_{02} are listed in tables S1 and S2 (see the SI in detail) together with κ_m and κ_h calculated from equations (18) and (19).

4.2. Dependency of relaxation parameters on mass fraction and pH

From the inspection of tables S1 and S2, there are significant differences among the three SPB suspensions (PS-PAA,

PS-PAA-1 and PS-PAA-2, see table 1) in relaxation parameters. Such differences are independent of the mass fraction of SPBs or the pH of the suspension. To clarify this, the parameters, $\Delta\varepsilon_1$, $\Delta\varepsilon_2$, $\Delta\kappa_1$, $\Delta\kappa_2$, τ_1 and τ_2 , are plotted against the mass fraction and pH in figures 5–7, respectively. As seen in figure 5(a), the dielectric increments (i.e. relaxation intensity, $\Delta\varepsilon_1$ and $\Delta\varepsilon_2$) of LF and HF relaxations for PS-PAA-1, PS-PAA-2 suspensions (red and green points, respectively; the same below) show the same change tendency and their values are close, while $\Delta\varepsilon_1$ and $\Delta\varepsilon_2$ of PS-PAA (blue points; the same below) are much greater than that of PS-PAA-1 and PS-PAA-2 in each SPB mass fraction. The results mean that the relaxation intensity for the LF or HF relaxation is mainly determined by the size of the PS core of SPBs, but has a little relation with the length of the PAA chain or the thickness of the soft layer. The relaxation intensity is proportional to the radius of the PS core, namely $\Delta\varepsilon \propto a$ (see figure 2 and table 1).

Interestingly, this result is not shown in the pH dependence of $\Delta\varepsilon_1$ and $\Delta\varepsilon_2$ for the three SPB suspensions when the pH of these suspensions changes from 3 to 11, as shown in figure 5(b). In acid media ($\text{pH} < 7$), the LF relaxation intensity $\Delta\varepsilon_1$ of PS-PAA is greater than that of PS-PAA-1 and PS-PAA-2, which also manifests $\Delta\varepsilon_1$ as proportional to the radius of the PS core. However, the change tendency of $\Delta\varepsilon_1$ for PS-PAA-1 and PS-PAA-2 with pH does not remain consistent because of the relaxation in density of the particle suspension. This is not only related to the radius of the PS core, but is also influenced by the soft layer consisting of PAA chains under various pH conditions. As previously mentioned in the introduction, the conformation of an annealed polyelectrolyte chain in the soft layer evidently depends on the pH of the medium. This is proved in the later discussions about figure 14, which show PAA chains gradually tend toward stretching with increasing pH. Thus, it is concluded that the gradual stretching of PAA chains with increasing pH causes a much greater thickness of the soft layer of PS-PAA-2 compared with PS-PAA-1 in the range of pH 3–11. This suggests $\Delta\varepsilon_1$ is proportional to d_s (soft-layer thickness), in spite of the positive correlation between the $\Delta\varepsilon_2$ for three kinds of SPBs

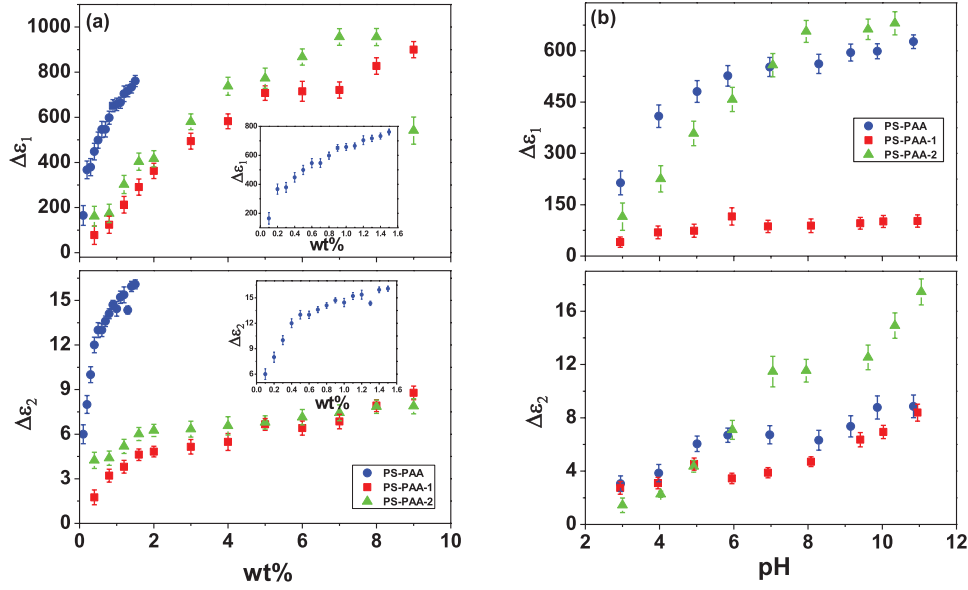


Figure 5. Mass-fraction dependence of the dielectric increment (a) and the pH dependence of the dielectric increment when the mass fraction of SPBs is 0.3% (b).

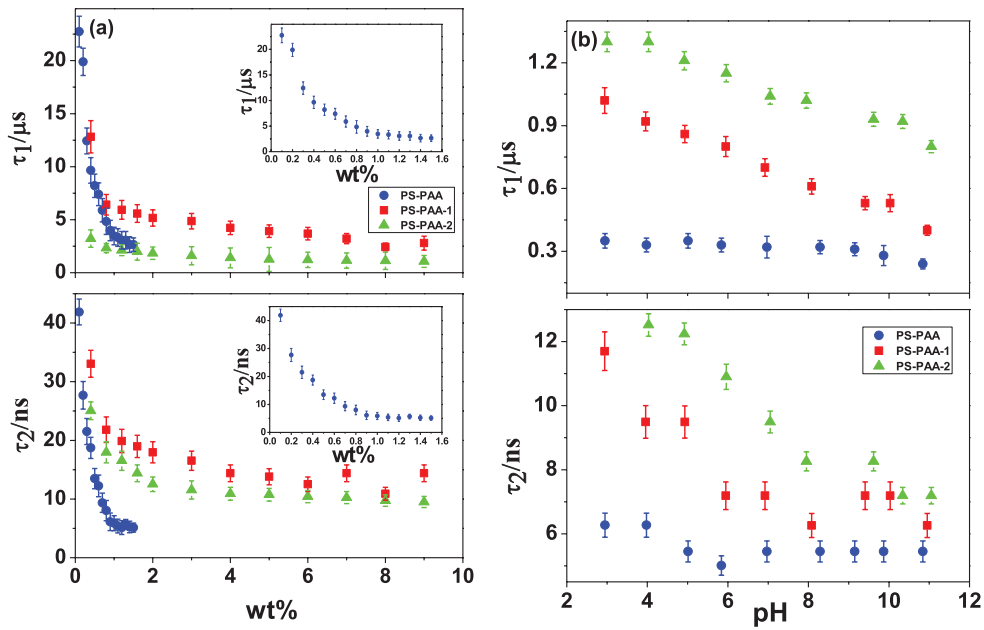


Figure 6. Mass-fraction dependence of the relaxation time (a) and pH dependence of relaxation time when mass fraction of SPBs is 0.3% (b).

(PS-PAA, PS-PAA-1 and PS-PAA-2) and the unobvious soft-layer thickness d_s (see figure 5(b)).

Figures 6(a) and (b) show the mass-fraction dependence and pH dependence of relaxation time τ_1 ($=1/2\pi f_{01}$) and τ_2 ($=1/2\pi f_{02}$) for the three kinds of SPB suspensions (PS-PAA, PS-PAA-1 and PS-PAA-2). It is obvious that both τ_1 and τ_2 for the three SPB suspensions decrease sharply in very low mass fraction (about 0.1%–6.0%) and then exhibit a significant platform. This suggests that when the number of SPB particles reaches a certain level, the charge distributions inside polyelectrolyte layer and at the interface between SPB particles and bulk solution became independent of the number of particles. This is because the relaxation time of interfacial

polarization depends mainly on the electrical properties of the interface or the constituent phases of a heterogeneous system. Similarly, τ_1 and τ_2 for PS-PAA-1 and PS-PAA-2 behave the same way in the experimental mass-fraction range including $\Delta\epsilon_1$ and $\Delta\epsilon_2$. Interestingly, the relaxation times of PS-PAA-1 SPBs with a relatively thin PAA layer (short-chain) are always slightly larger than PS-PAA-2 SPBs of thicker PAA layers (long-chain). Note that under the same mass fraction, the bigger the size of the SPB particle the fewer the SPB number needed to reach the same mass fraction, i.e. the larger size of particle requires a fewer number for the same volume fraction. From figure 6(a), we can roughly see that the relaxation time and the radius of SPB R_s demonstrate a negative

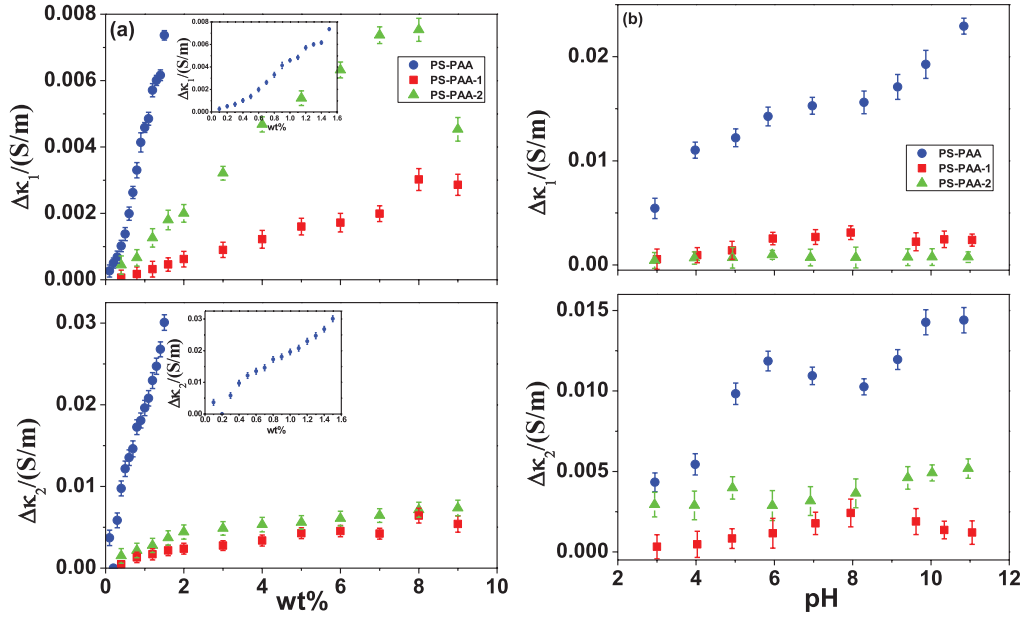


Figure 7. Mass-fraction dependence of the conductivity increment (a) and the pH dependence of the conductivity increment when the mass fraction of SPBs is 0.3% (b).

correlation (see figure 2). A slightly different result is found in the pH dependence of the LF and HF relaxation times, τ_1 and τ_2 , shown in figure 6(b). It is clear that for the same pH, the relaxation times τ_1 and τ_2 are determined by the radius of the PS microsphere instead of SPBs in a sequence which is $\tau_{1 \text{ or } 2}$ (PS-PAA-2) > $\tau_{1 \text{ or } 2}$ (PS-PAA-1) > $\tau_{1 \text{ or } 2}$ (PS-PAA). This means that the relaxation times and the radius of PS a show a negative correlation. The biggest difference in the two results shown in figures 6(a) and (b) is that the values of τ_1 and τ_2 for the same PS core with different chain length are different. This reflects the fact that the relaxation time is also related to the structural and electrical properties of the polyelectrolyte layer, and the layer is influenced by the pH of bulk solution.

In regard to the conductivity increment $\Delta\kappa_1$ and $\Delta\kappa_2$, in essence they are not independent and are closely related to dielectric increment $\Delta\varepsilon_1$ and $\Delta\varepsilon_2$ as defined by equations (17) and (18). Therefore, they behave in the same way as the dielectric increment shown in figures 7(a) and (b). It is worth stressing that the values of $\Delta\kappa_1$ and $\Delta\kappa_2$ for PS-PAA are much larger than that of PS-PAA-1 and PS-PAA-2, revealing that the conductivity increment is positively correlated with the size of PS microsphere. In addition, the number of counterions is proportional to the SPBs' mass fraction, hence, $\Delta\kappa \propto \text{wt}_{\text{SPB}}\%$.

4.3. Theoretical analysis of dielectric spectroscopy based on the G–Z model

According to the method mentioned in section 2, the parameters (called ‘phase parameters’ in this work) reflecting the electrical properties and structural features of the constituent phases (PS core, shell phase (polyelectrolyte layer) and external medium) of the SPB suspensions are obtained by fitting equations (1)–(7) to the observed dielectric spectra (as shown in tables 2, 3, S3 and S4, with some parameter values relevant to SPB suspensions and the experimental conditions:

Table 2. Calculated phase parameters for PS-PAA SPB suspensions of different mass fractions based on the spherical-shell model.

wt%	ε_i	ε_s	ε_a	κ_s (S m ⁻¹)	Φ (%)	ζ (mV)
1.5	2.5	77.2	78	0.15	6.3	−20.0
1.3	2.5	77.6	78	0.13	3.6	−22.1
1.1	2.5	78.0	78	0.11	2.8	−22.3
1.0	2.5	78.2	77	0.11	2.4	−22.6
0.9	2.5	78.4	77	0.10	2.1	−22.7
0.7	2.5	78.6	75	0.09	1.3	−23.0
0.5	2.5	78.9	76	0.08	0.8	−23.2
0.3	2.5	79.4	76	0.06	0.4	−23.4
0.1	2.5	79.8	76	0.05	0.2	−23.5

Table 3. Calculated phase parameters for 0.3% PS-PAA SPB suspensions of varying pH based on the spherical-shell model.

pH	ε_i	ε_s	ε_a	κ_s	Φ (%)	ζ (mV)	d_s (nm)	v
2.95	2.5	78.4	75	0.11	7.3	−38.0	176.0	7.19
3.98	2.5	78.4	75	0.11	7.6	−39.5	179.0	6.98
5.01	2.5	76.5	75	0.13	3.6	−40.0	216.0	4.95
5.84	2.5	76.4	78	0.14	7.8	−41.2	217.0	4.90
6.97	2.5	76.3	76	0.14	8	−42.0	219.0	4.82
8.29	2.5	76.3	78	0.14	8.1	−42.1	219.5	4.80
9.15	2.5	76.7	77	0.14	8.1	−42.1	219.5	4.80
9.87	2.5	77.2	77	0.14	8.1	−42.2	219.5	4.80
10.84	2.5	77.5	73	0.14	8.1	−42.3	219.0	4.82

$T = 298$ K, $D = 6.72 \times 10^{-9}$ m² s⁻¹ and η (the viscosity of the medium) = 8.904×10^{-4} Pa · s [40]. Figure 8 shows an example of best-fit curve: the frequency dependence of the permittivity for PS-PAA SPB suspension at $\text{wt}_{\text{SPB}}\% = 0.1\%$ (hollow black circles) and at pH = 2.95 (hollow red circles), and the solid lines are the best-fit curves by equations (1)–(7).

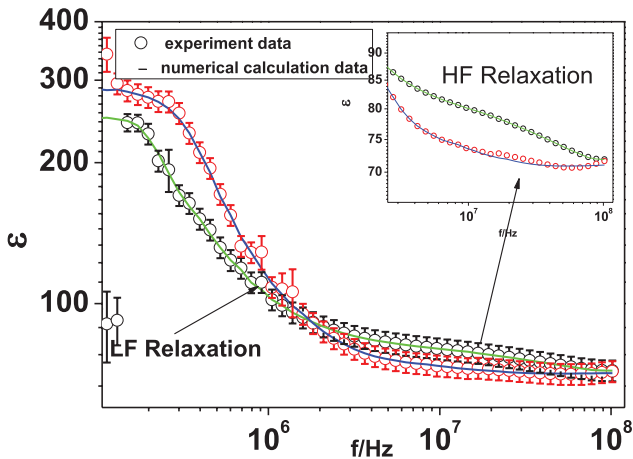


Figure 8. Frequency dependence of permittivity for the PS-PAA SPB suspensions at $wt_{SPB}\% = 0.1\%$ (hollow black circles) and at $pH = 2.95$ (hollow red circles): hollow circles, experimental permittivity data after depolarization; solid line, the best numerical calculation data by equations (1)–(7). The inset shows an expanded view of the HF dispersion with the best numerical curves.

4.3.1. Chain conformation of brush layer with different chain length. Figures 9 and 10 respectively show the SPBs’ mass fraction, pH dependence of permittivity of the PS core (ϵ_i), polyelectrolyte layer (soft-shell phase) (ϵ_s) and external medium (ϵ_a) for PS-PAA, PS-PAA-1 and PS-PAA-2 kinds of SPB suspensions. The permittivity of the PS core is 2.5. This is very close to a bare PS microsphere and independent of the number of SPBs and pH of the medium, as shown in figures 9(a) and 10(a). We focus on the shell phase, i.e. polyelectrolyte layer: whether changing the SPBs’ mass fraction or altering the pH, the ϵ_s of the PS-PAA-1 is relatively larger (105–120), while the ϵ_s of PS-PAA and PS-PAA-2 is between 72 and 78 (figures 9(b) and 10(b)), which is close to ϵ_a of the external medium. The difference in ϵ_s among the three kinds of SPBs (PS-PAA-1, PS-PAA and PS-PAA-2) suggests that magnitude of ϵ_s is mainly determined by the length of the polyelectrolyte chains in the shell phase, while it has a little relation to the size of the PS core (see table 1 and figure 2). A detailed discussion now follows.

The average value of permittivity of the PS-PAA and PS-PAA-2 in figure 9(b) or in figure 10(b) ranges from 66 to 78, which is slightly less than pure water ($\epsilon_{water} = 78.35$, 298 K). In general, the water composition in the polyelectrolyte layer is approximated to 90%. Therefore, the permittivity of the PAA layer for PS-PAA and PS-PAA-2 is reasonable. However, the permittivity of the PAA layer of PS-PAA-1, which is about 110–120 is much larger than PS-PAA and PS-PAA-2. This implies that a huge apparent dipole moment exists among the PAA chain layer of PS-PAA-1 SPBs. It originates from a strong orientational order of water molecules in the PAA layer and leads to an intriguingly high permittivity of about 110–120. The strong orientational order of water molecules from the hydrogen-bond interaction between the carboxyl groups on PAA chains and water molecules, is more likely to occur in the shorter PAA chains. However, for the longer polymer chain with a higher flexibility, the water

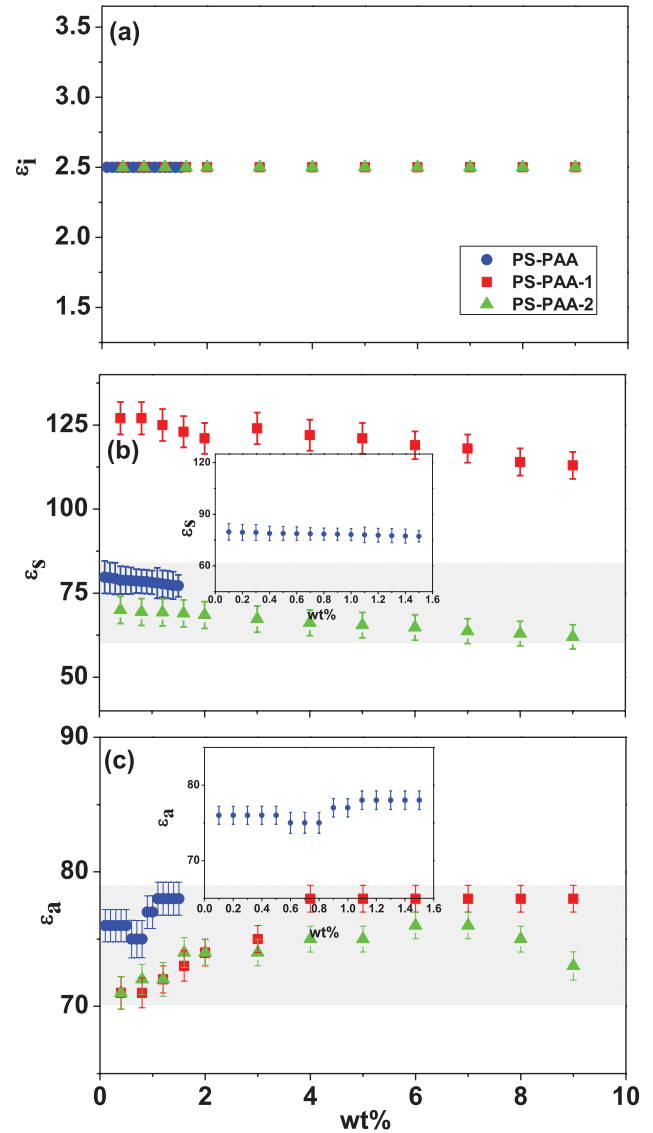


Figure 9. Mass-fraction dependence of the permittivity of the PS core (ϵ_i) (a), soft layer (or shell phase) (ϵ_s) (b) and external medium (ϵ_a) (c) for three kinds of SPB (PS-PAA, PS-PAA-1 and PS-PAA-2) suspensions.

molecules (hydrogen bond) arranges randomly in the polyelectrolyte layer because of the flexibility of the chains. As a result, no apparent additional macro-dipole moment is formed (as shown in figure 11). As can be seen in figures 9(b) and 10(b), the permittivities of the PAA layer for PS-PAA and PS-PAA-2 are both slightly less than pure water.

The high permittivity of the PAA layer of PS-PAA-1 SPBs can be interpreted from microcosmic point of view. According to the research by Allen and Ballenegger [53, 54], the image-charge interactions exists in the interface where dielectric discontinuity exists between the two substances with different permittivities, such as polar solution and polymer chain. Essentially, the image-charge interaction originates in the arrangement of water molecules at the interface. The arrangement is normally recognized as the first layer of water molecules to align their dipoles parallel to the interface in terms of electrostatic interactions of these dipoles with their images.

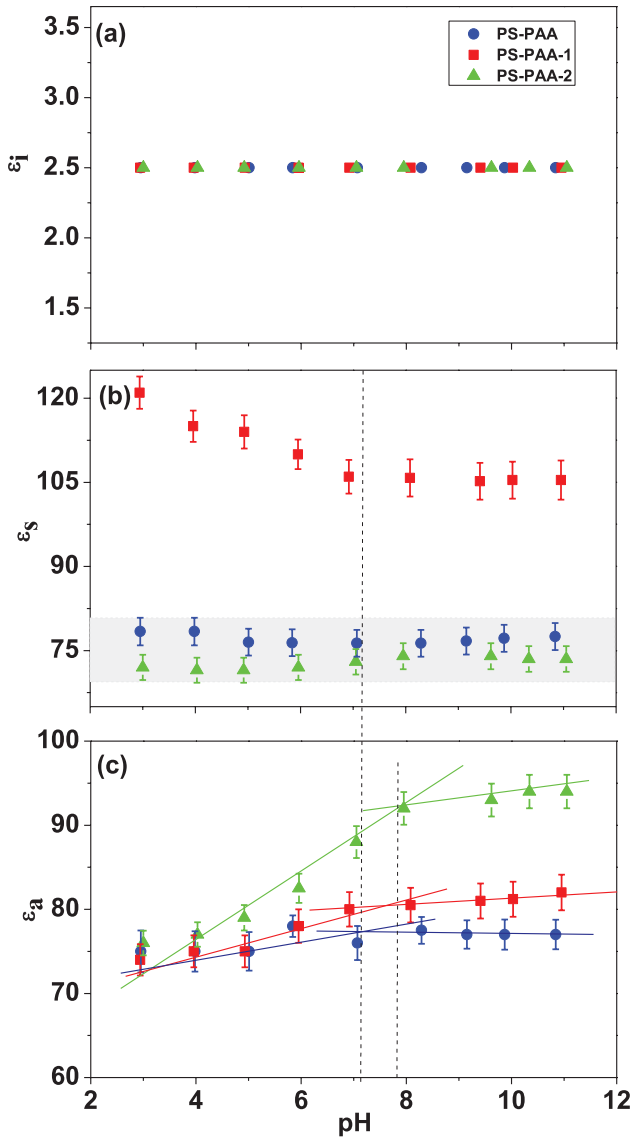


Figure 10. The pH dependence of the permittivity of the PS core (ϵ_i) (a), soft layer (or shell phase) (ϵ_s) (b) and continuous medium (ϵ_a) (c) for three kinds of SPB (PS-PAA, PS-PAA-1 and PS-PAA-2) suspensions when the mass fraction of SPBs is 0.3%.

Following this, there is a large dielectric discontinuity between water and the PAA chain in the brush layer. The water molecules alongside the PAA chains align their dipoles parallel to the hydrophobic chains as illustrated in figure 11 (see the caption for details). A larger value of dipole–dipole correlations (between red arrows and blue arrows) is favorable, as shown in figure 11. As a result, a high permittivity appears in the PAA polyelectrolyte layer for the PS-PAA-1 SPBs. This explanation concerning water molecule orientation is well supported by the works of Gawrisch. He found that the water molecules in the hydrophobic interface have a compact orientational orderliness. Therefore, the highly ordered molecules interact with the carbonyl dipoles of dipalmitoylphosphatidylcholine and contribute to the dipole potential [55].

Besides the flexible chain conformation, the carboxyl dipoles (or carbonyl dipoles at higher pH) on the PAA

chains also contribute to the dipole moment (see red arrows in figure 11). This part of the dipole moment also influence the permittivity ϵ_s or polarity of the brush layer [55–57]. As illustrated in figure 11(b), in the soft layer of PS-PAA or PS-PAA-2, the dipoles between carboxyl groups present a disorderly orientation without an apparent dipole moment, while the orientation of the dipoles in the shorter PAA chain layer presents more order (figure 11(a)). The orientational order of water and the intrinsic dipoles of the carboxyl group (or carbonyl group at higher pH) result in the consequences shown in figures 9(b) and 10(b): the layer permittivity ϵ_s of PS-PAA-1 with a shorter chain is much larger than PS-PAA and PS-PAA-2 with longer polyelectrolyte chains.

4.3.2. Anomalous permittivity of water in alkaline media. The permittivity of external medium ϵ_a , which is calculated using equations (1)–(7) remains almost the same with the mass fraction of SPBs. Values of ϵ_a for the three suspensions, around 78 (figure 9(c)), are very close to water at 298 K ($\epsilon_{\text{water}} = 78.35$), showing the number of SPBs has limited impact on the polarity of external solutions of suspension. This also verifies the rationalities of the model used in this work. However, when the acid–base property, i.e. the pH of these suspensions is changed, the calculated permittivities of the external solutions ϵ_a are no longer a constant. In other words, the ϵ_a values for the three suspensions (PS-PAA, PS-PAA-1 and PS-PAA-2) change with pH; this is notable PS-PAA-2, as shown in figure 10(c). Normally ϵ_a of the acid medium is less than alkaline media. This implies that an extraordinary non-covalent-bond-associated structure of water molecules, which is an unsymmetrical oligomer of water clusters, forms in an alkaline medium because of its bigger dipole moment. The dipole moment of strong symmetric water was reported to be very low [58]. Hence, the structural water in alkaline media most likely has a higher polarity and larger permittivity than usual water clusters.

4.3.3. Migration of counterions in the brush layer. The conductivities of the polyelectrolyte brush layer κ_s for three kinds of SPBs (PS-PAA, PS-PAA-1 and PS-PAA-2) in tables 2, 3, S3 and S4 are plotted as a function of SPBs’ mass fraction or the pH in figure 12. It is reasonable to assume that in a low-salt medium, κ_s is dominated by the diffusion and migration of the counterions along the polyelectrolyte chains. The brush-layer conductivity κ_s of the three different brush thickness increases in different ways as their respective mass fractions increase (figure 12(a)). Thus, the conductivity variation in the polyelectrolyte chain layer is not only from the diffusion of the counterions along the chain, but is also determined by some complex electrical conduction mechanisms that are closely related to the thickness of polyelectrolyte layer and the chain conformation.

As the pH of the suspensions varies, the conductivities of the polyelectrolyte brush layer κ_s for the three SPBs transform in a similar way as the mass of the SPBs. As shown in figure 12(b), the values of κ_s for the three SPBs increase with an increasing pH, which indicates that reducing the acidity of the suspensions enhances the migration of the counterions

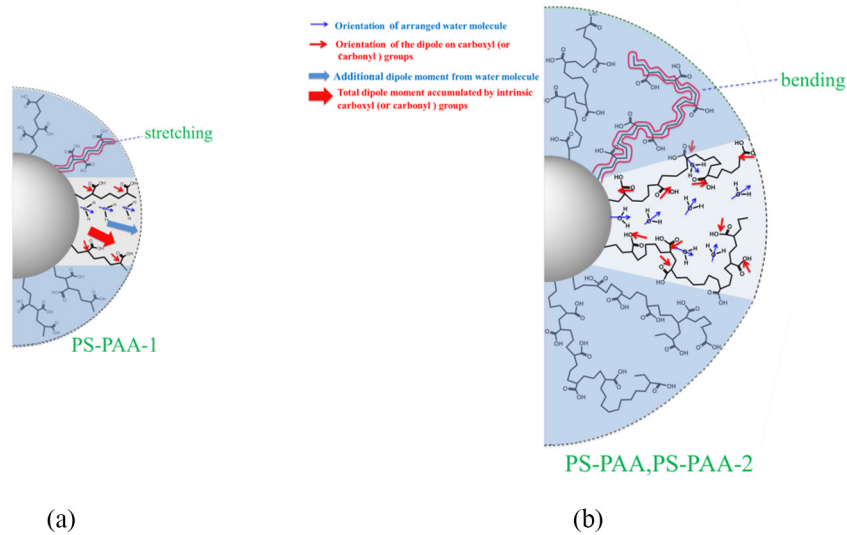


Figure 11. Schematic of the arrangement of water molecules along hydrocarbon chains in the brush layer of PS-PAA-1 (short-chain) (a) and that of PS-PAA, PS-PAA-2 (long-chain) (b). As shown in the scheme, the water molecule alongside the PAA chains align their dipoles parallel to the hydrophobic chains because of the dielectric discontinuity between the water and PAA chains, and the orientational ordering of water dipoles accumulate a huge apparent dipole (bold blue arrow) resulting in a huge permittivity of the shell phase for PS-PAA-1 (the shorter the polyelectrolyte chain is, the more orderly it will be arranged in the shell phase) and the intrinsic dipoles of the carboxyl group (or carbonyl group at higher pH) can also contribute to the total dipole moment (bold red arrow). The size of the arrow is not equal to the contribution to the total dipole moment.

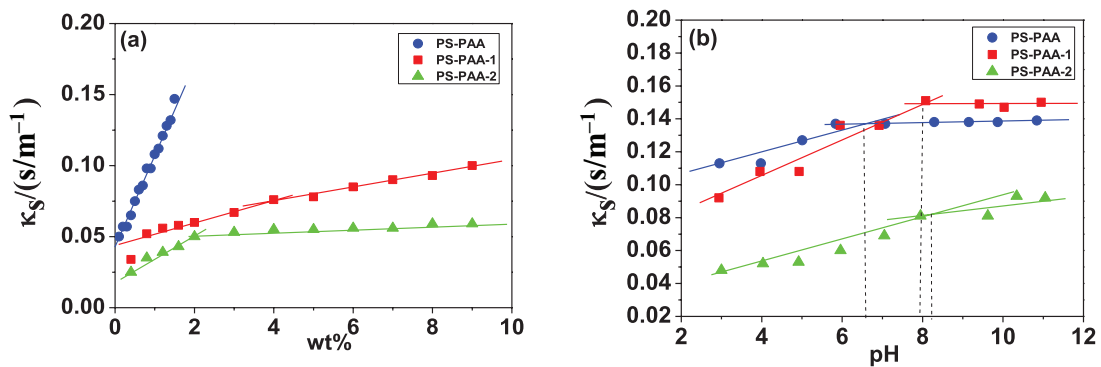


Figure 12. Mass-fraction dependence of conductivity of soft layer (or shell phase) (κ_s) for three kinds of SPB (PS-PAA, PS-PAA-1 and PS-PAA-2) suspensions (a) and pH dependence of conductivity of soft layer (or shell phase) (κ_s) for three kinds of SPB (PS-PAA, PS-PAA-1 and PS-PAA-2) suspensions when the mass fraction of SPBs is 0.3% (b).

along the PAA chains and results in an increase in conductivity of the brush layer. From the point of view of the deprotonation and electric neutrality, this can be interpreted in the following way: lowering the acidity of suspensions causes the H⁺ on the carboxyl groups in PAA chains to decrease and fixed charge density to accumulate in the soft layer. Consequently, some charged sites are generated with more counterions K⁺ permeating and becoming confined in the brush layer. Under external AC electrical field the fluctuations of these counterions around fixed charges on the PAA chain increase κ_s [14]. It is worth noting that the three κ_s -pH curves have obvious inflection: the rates of increase of κ_s for the three systems are inhibited when pH > 7 remains constant. Considering [34] the deformation of the chain conformation in the brush layer of SPBs induced by the alternative pH as well as collapse or stretch, full swelling (or full collapsing) of the polyelectrolyte brush layer generates such a platform of κ_s . No matter whether the layers fully stretch or collapse or not, the thickness of the

brush layer remains unchanged when pH > 7. Consequently, the conductivity of the brush layer is a constant. It will be further clarify in this work that the PAA chains of anionic SPBs fully stretch in alkaline medium.

4.3.4. Stretch of polyelectrolyte brushes in alkaline medium.

The volume fraction Φ of SPBs for three suspensions in different pH is numerically calculated based on equations (1)–(7), and plotted against pH in figure 13. It needs to be noted that Φ also depends on the acidity of the solution medium just like in the case of conductivity κ_s of the brush layer (figure 12(b)). This pH response is a typical feature of the annealed brushes. Interestingly, in alkaline or strong alkaline medium, the volume fraction likewise remains unchanged as well as κ_s . From the configuration of SPBs illustrated in figure 2, it is clear that the change of SPB volume fraction depends entirely on the thickness of the brush layer because the PS core is unchanging. This can be further verified by the result of figure 13(b)

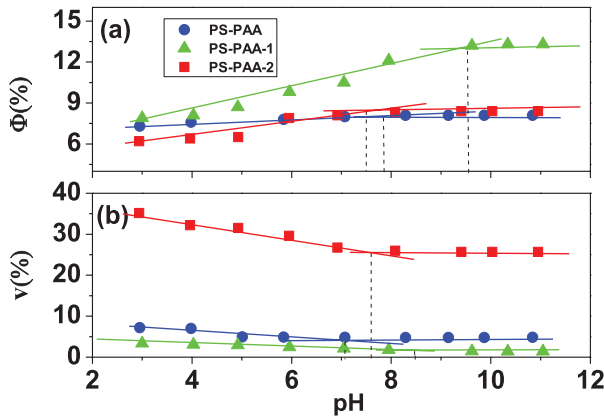


Figure 13. pH dependence of volume fraction Φ of SPBs in the systems (a) and the pH dependence of volume fraction ν of PS core in the whole SPB particles (b) for three kinds of SPB (PS-PAA, PS-PAA-1 and PS-PAA-2) suspensions when the mass fraction of SPBs is 0.3%.

where the pH dependence of the volume fraction ν of the PS core presents a completely opposite change trend, which shows a good agreement with the model (figure 1) and the configuration of SPB (figure 2). Therefore, the increase of Φ in a neutral or weakly basic medium indicates polyelectrolyte PAA chains stretches, i.e. the brush layer swells, while the unaltered Φ in a range of about 8–11 pH means that the PAA chains in the brush layer always remain well extended in stronger alkaline medium.

The thickness d_s of the spherical shell of SPBs in model, which is calculated simultaneously using equations (1)–(7), directly reflects the change of chain conformation in the polyelectrolyte layer at different acidity–alkalinity ranges. Figure 14 shows the pH dependence of d_s for three SPBs (PS-PAA, PS-PAA-1 and PS-PAA-2) at an SPB mass fraction of 0.3%. The thickness d_s increases with an increase of pH in acid medium for PS-PAA, PS-PAA-1 and in acid and weak alkaline medium for PS-PAA-2, and then reaches its respective steady value. A study of the interaction between PAA brushes, as measured by optical tweezers and independent ellipsometric measurements, has been reported by Kremer *et al* [59]. The study showed that the increase of the brush length is caused by the pH-induced augment of the PAA dissociation and results in a stretching of the grafted chains. The same result has been illuminated by laser light scattering [4], from which the rationality of the model and numerical calculation used in this work are reaffirmed.

The reasons that the shell thickness d_s varies with the pH of solution can be explained as follows: the variation of d_s is controlled by the dissociation degree of carboxyl groups on PAA chains. Due to the small the dissociation degree at lower pH, there is less charge on the chains and weak electrostatic repulsion between the chains. Hence, the chains tend to collapse and lead to less d_s . As pH rises, the charges on the chains increase gradually with a large electrostatic repulsion. As a result, PAA chains within the brush layer tend to stretch and the brush layer thickens. Moreover, more counterions

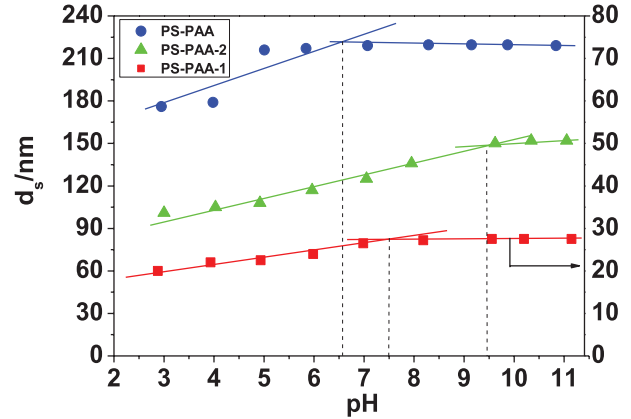


Figure 14. pH dependence of shell thickness d_s for three kinds of SPB (PS-PAA, PS-PAA-1 and PS-PAA-2) suspensions when the mass fraction of SPBs is 0.3%.

in the bulk solution permeate into the brush layer driven by Donnan potential because of higher electric charges in the layer. Hence, there is a high osmotic pressure within the brush layer. These two effects keep the shell phase in the swollen state [60–62]. When pH is raised up to a certain value, the carboxyl group on the PAA chains are fully deprotonated and the electrostatic repulsion among the negatively charged polyelectrolyte chains reaches the maximum. The conformation of PAA chains in the layer are no longer affected by pH and shell thickness and d_s is kept at a constant, as shown in figure 14. The above analyses can be confirmed by a study in which electrostatic interactions within the brush layer are screened at high ionic strength, and the brush has no response to pH [4].

4.3.5. Zeta potential (ζ -potential) of SPB surface. It is well known that the stability of colloid particles depends on the net charge of the particle surface. To evaluate the net charge of the particle surface, including the PAA SPBs, ζ -potential is a key parameter. The ζ -potential of PAA SPB particles is zero due to the dissociation of the monomer of PAA chains. Since the suspended SPB colloidal particle is regarded as an ideal spherical-shell structure, its ζ -potential can be calculated using equations (1)–(7) as described previously. Figures 15(a) and (b) depict the mass-fraction dependence and pH dependence of ζ -potential, respectively, for the three SPB suspensions (see tables 2, 3, S3 and S4 for the values of ζ -potential). The ζ -potential decreases with an increase in the mass fraction of SPBs, as ζ -potential is related to the degree of dissociation of PAA chains. According to Le Châtelier's principle [63], less mass fraction promotes the dissociation of the carboxyl groups on PAA chains. As a result, more charges generated in the shell phase, which consists of PAA polyelectrolyte chains, increase ζ -potential. Thus, the ζ -potential of PS-PAA SPBs is much greater than PS-PAA-1 and PS-PAA-2, even though the mass fraction of PS-PAA is lower. On the contrary, the ζ -potential for three kinds of SPB (PS-PAA, PS-PAA-1 and PS-PAA-2) suspensions increases as pH rises until pH rises above eight, due to the completeness of the deprotonation of the carboxyl groups on PAA chains in alkaline medium [4].

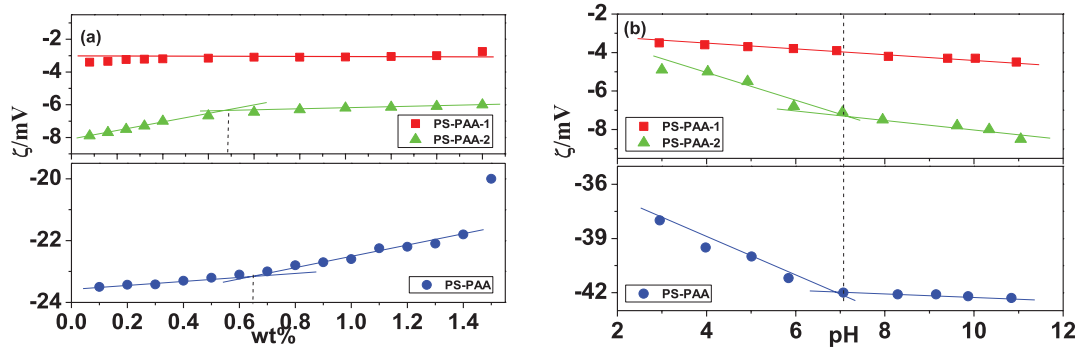


Figure 15. Mass-fraction dependence of zeta potential of SPB particles for three kinds of SPB (PS-PAA, PS-PAA-1 and PS-PAA-2) suspensions (a) and pH dependence of zeta potential of SPB particles for three kinds of SPB (PS-PAA, PS-PAA-1 and PS-PAA-2) suspensions when the mass fraction of SPBs is 0.3% (b).

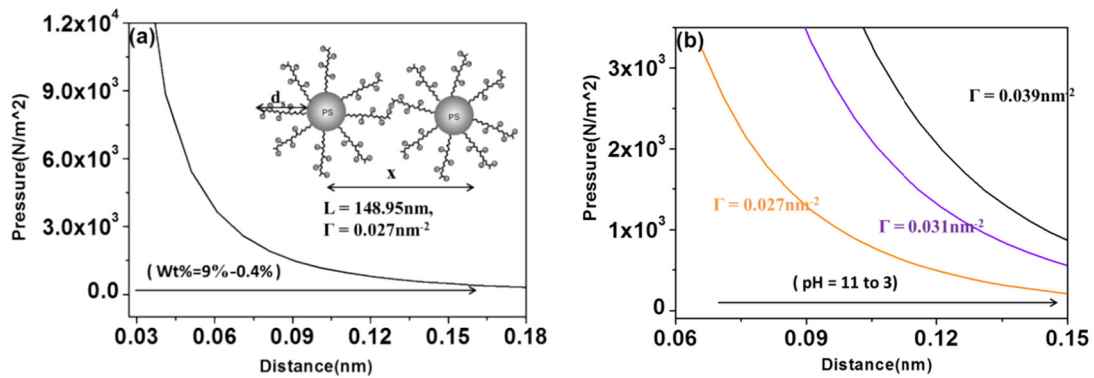


Figure 16. Disjoining pressure between two similar SPB-particle-grafted PAA chains in PS-PAA-2 suspension. The parameters used for the calculation by equation (21) are $d_s = 148.95 \text{ nm}$ and Γ (approximate) $= 0.027 \text{ nm}^{-2}$ [4] under different mass fractions (a) and the shell-phase thickness d_s for PS-PAA-2 (with three grafting densities $\Gamma = 0.027 \text{ nm}^{-2}$, 0.031 nm^{-2} , 0.039 nm^{-2} , see table (1) in [4]) under different pH values (b).

4.3.6. Force between PAA chains grafted onto the particle surface. In general, the surface charge of a colloidal particle can generate repulsion energy between the particles, and the ζ -potential on the particle surface can also impact on the repulsive force and the stability of the whole suspension [13, 64]. Some researchers reported that a colloidal suspension is stabilized by the adsorption of polymer molecules onto the particles of the suspension [9, 65]. For the present SPB particle suspension, the stabilizing effect is achieved by the steric repulsive force between the grafted polyelectrolyte chains on the SPB surface as well as the electrostatic interactions.

To the best of our knowledge, there is no simple, comprehensive theory about steric forces to describe soft-particle systems due to their complex composition. The most important interaction among steric forces, the repulsive force, originates from the configuration entropy of the polymer chains. When two polymer-coated particles approach, the reduction in the number of available configurations of the polymer chains gives rise to an ‘entropic’ repulsive force [66]. The repulsion force $\Pi(x)$ among the particle surfaces formed by densely grafting linear polyelectrolyte chains follows the expression proposed by de Gennes [67]:

$$\Pi(x) = \kappa_B T \Gamma^{3/2} \left[\left(\frac{2d_s}{x} \right)^{9/4} - \left(\frac{x}{2d_s} \right)^{3/4} \right] \quad (21)$$

where κ_B is the Boltzmann constant, T is the absolute temperature, Γ is grafting density in number of molecules per unit area, x is the distance between two separated colloidal particles, and d_s is the thickness of the brush layer.

Figure 16(a) shows that the repulsion for PS-PAA-2 suspension changes as a function of inter-particle distance (mass fraction of SPBs), which is calculated using equation (21) with $d_s = 148.95 \text{ nm}$ ($\Gamma = 0.027 \text{ nm}^{-2}$ was obtained from the literature [4]). The repulsion interactions among the PS-PAA-2 SPB particles is most likely stronger upon approaching the SPB particles, which is similar with the result reported by de Gennes *et al* [67]. This observation can be explained by the overlapping and associating of stretched polyelectrolyte chains, which is larger upon increasing the mass fraction. Follow this explanation, the repulsion among polyelectrolyte chains from neighbor SPBs should be influenced by pH. To illuminate the repulsion force versus the pH values for PS-PAA-2, an SPB suspension with different grafting densities is depicted in figure 16(b). It can be clearly seen that the repulsion enhances significantly with the increase of pH and is proportional to the grafting density. With pH increasing, the PAA chains become more and more stretched, which enhances the overlapping and associating among PAA chains from neighbor SPBs. Such observation demonstrate good agreement with the previous discussion in section 4.3.4. Therefore,

with two PS-PAA-2 approaching, the entropic repulsive force among SPBs become stronger and stronger. Similar results in relation to the interaction force between PAA brushes [59] or poly(2-vinylpyridine) brushes [68] are reported by Kremer *et al.* Their optical-tweezer measurement demonstrated that the interaction of polyelectrolyte brushes is dominated by entropic forces resulting from the counterions inside the brush layer. The force–distance curves was quantitatively described by the Jusufi model which also takes into account the entropic effect of the confined counterions. From the results of figure 16 and the analysis above, the conclusion can be drawn that lowering the acidity of the solution (i.e. raising pH) or increasing the number of SPBs (i.e. increasing the concentration of SPBs) improves the stability of the colloidal dispersion.

5. Conclusions

The dielectric behavior of three PS-core PAA SPB suspensions at varying SPB concentrations and pH is systematically studied in a frequencies ranging from 40 Hz to 110 MHz. Two unique relaxations are clearly identified. A spherical-shell dielectric model characterizing the structure and electrical properties of the constituent phases of SPBs is applied to quantitatively calculate the conductivity, permittivity, and thickness of the brush layer as well as the electrical properties of the solution with the relaxation parameters obtained from the fitting of the H–N equation. In particular, the ζ -potential of the SPB particle surface is determined simultaneously in this computing. The electrical properties of the core, brush layer, and external medium of the SPB suspension are quantified by modeling analysis for the first time.

Through analyzing the mass-fraction dependence and pH dependence of the relaxation parameters/phase parameters for three SPB suspensions, it is found that the chain conformation of PAA in the brush layer depends mainly on the acidity of the solution (i.e. pH), and the stretching of the chains remains relatively steady in alkaline medium. This result is consistent with previous experimental studies into SPBs. It is concluded that the model and calculation method used in this work are suitable for the SPB suspension. In addition, the existence of additional dipole moments in shorter PAA chains is revealed by the abnormal permittivity of the shell phase of PS-PAA-1 SPBs with a shorter PAA chain. The results of the conductivity for three kinds of SPBs suggest that the migration of counterions in the brush layer is affected dramatically by the thickness of the brush or chain conformation.

The calculated ζ -potential values indicate the amount of net charge of PAA brush layers with different thicknesses. The result of the pH dependence of ζ -potential supports the conclusion derived from the phase-parameter dependence of pH or the mass fraction mentioned in this work. Theoretical simulation of the repulsive force among SPB particles correlates pH or SPB concentration with the colloid stability: lowering the acidity of the solution or increasing the concentration of SPBs improves the stability of the colloidal dispersion. This finding may provide clues for the further application of SPB dispersions in many disciplines.

Acknowledgments

The authors wish to thank Prof. Xuhong Guo (State Key Laboratory of Chemical Engineering, East China University of Science and Technology, China) for supplying the SPBs sample. The financial support from the National Natural Scientific Foundation of China (No. 21173025, 21473012) and the Major Research Plan of NSFC (No. 21233003) are also gratefully acknowledged.

Supporting information description

The Supporting Information contains relaxation parameters (ε_b , ε_m , ε_h , f_{01} , f_{02} , κ_b , κ_m and κ_h). The Supporting Information is available free of charge via the internet at: stacks.iop.org/JPhysCM/29/055102/mmedia

Appendix

The quantities S and d_{Lh} in equation (4), given by Grosse and Zimmerman, are simplified by assuming a 1–1 electrolyte that has the same diffusion constant D for the anion and cation.

$$S = \frac{2(R^+ + R^- + 4)}{(R^+ + 2)(R^- + 2 - U) + (R^- + 2)(R^+ + 2 - U)} \quad (\text{A.1})$$

$$d_{Lh} = \frac{R^+ + R^- - 2}{R^+ + R^- + 4} \quad (\text{A.2})$$

$$R^\pm = \frac{1}{K_D R_s} [4(e^{\mp \tilde{\zeta}/2} - 1)(1 + 3m) \pm 6m\tilde{\zeta}]. \quad (\text{A.3})$$

The reciprocal Debye screening length $K_D = \sqrt{2F^2 c_a / (RT \varepsilon_a \varepsilon_0)}$

$$U = \frac{48m}{K_D R_s} \ln \left[\cosh \left(\frac{\tilde{\zeta}}{4} \right) \right]. \quad (\text{A.4})$$

The dimensionless zeta potential is given by $\tilde{\zeta} = F\zeta / (RT)$

$$m = \frac{2\varepsilon_a \varepsilon_0 \left(\frac{RT}{F} \right)^2}{3\eta D}, \quad (\text{A.5})$$

η is the viscosity of the medium.

The conductivity of the external medium κ_a is given by $\kappa_a = 2DF^2 c_a / (RT)$.

References

- [1] Guo X, Weiss A and Ballauff M 1999 Synthesis of spherical polyelectrolyte brushes by photoemulsion polymerization *Macromolecules* **32** 6043–6
- [2] Ballauff M 2007 Spherical polyelectrolyte brushes *Prog. Polym. Sci.* **32** 1135–51
- [3] Gu S *et al* 2015 Kinetic analysis of the reduction of 4-nitrophenol catalyzed by Au/Pd nanoalloys immobilized in spherical polyelectrolyte brushes *Phys. Chem. Chem. Phys.* **17** 28137–43
- [4] Guo X and Ballauff M 2001 Spherical polyelectrolyte brushes: comparison between annealed and quenched brushes *Phys. Rev. E* **64** 051406

- [5] Wittemann A, Haupt B and Ballauff M 2003 Adsorption of proteins on spherical polyelectrolyte brushes in aqueous solution *Phys. Chem. Chem. Phys.* **5** 1671–7
- [6] Lu Y *et al* 2007 *In situ* formation of Ag nanoparticles in spherical polyacrylic acid brushes by UV irradiation *J. Phys. Chem. C* **111** 7676–81
- [7] Guo X and Ballauff M 2000 Spatial dimensions of colloidal polyelectrolyte brushes as determined by dynamic light scattering *Langmuir* **16** 8719–26
- [8] Wittemann A *et al* 2005 High elongation of polyelectrolyte chains in the osmotic limit of spherical polyelectrolyte brushes: a study by cryogenic transmission electron microscopy *J. Am. Chem. Soc.* **127** 9688–9
- [9] Pincus P 1991 Colloid stabilization with grafted polyelectrolytes *Macromolecules* **24** 2912–9
- [10] Schneider C *et al* 2010 Stability behavior of anionic spherical polyelectrolyte brushes in the presence of La (III) counterions *Phys. Rev. E* **82** 011401
- [11] Irigoyen J *et al* 2013 Spherical polyelectrolyte brushes' constant zeta potential with varying ionic strength: an electrophoretic study using a hairy layer approach *Soft Matter* **9** 11609–17
- [12] Jusufi A, Likos C and Ballauff M 2004 Counterion distributions and effective interactions of spherical polyelectrolyte brushes *Colloid Polym. Sci.* **282** 910–7
- [13] Hoffmann M *et al* 2009 Surface potential of spherical polyelectrolyte brushes in the presence of trivalent counterions *J. Colloid Interface Sci.* **338** 566–72
- [14] Dukhin S S, Zimmermann R and Werner C 2004 Intrinsic charge and Donnan potentials of grafted polyelectrolyte layers determined by surface conductivity data *J. Colloid Interface Sci.* **274** 309–18
- [15] Dukhin S S, Zimmermann R and Werner C 2007 Surface conductivity reveals counterion condensation within grafted polyelectrolyte layers *J. Phys. Chem. B* **111** 979–81
- [16] Dukhin S S, Zimmermann R and Werner C 2008 Charge density distribution at interfaces between polyelectrolyte layers and aqueous solutions—experimental access and limitations of traditional electrokinetics *J. Colloid Interface Sci.* **328** 217–26
- [17] Füllbrandt M, von Klitzing R and Schönhals A 2013 The dielectric signature of poly (*N*-isopropylacrylamide) microgels at the volume phase transition: dependence on the crosslinking density *Soft Matter* **9** 4464–71
- [18] Madkour S *et al* 2015 Calorimetric evidence for a mobile surface layer in ultrathin polymeric films: poly (2-vinyl pyridine) *Soft Matter* **11** 7942–52
- [19] Grosse C *et al* 1998 Broad frequency range study of the dielectric properties of suspensions of colloidal polystyrene particles in aqueous electrolyte solutions *J. Colloid Interface Sci.* **205** 26–41
- [20] Grosse C and Delgado A 2010 Dielectric dispersion in aqueous colloidal systems *Curr. Opin. Colloid Interface Sci.* **15** 145–59
- [21] Jiménez M L *et al* 2011 Giant permittivity and dynamic mobility observed for spherical polyelectrolyte brushes *Soft Matter* **7** 3758–62
- [22] Ahualli S *et al* 2012 Electrophoresis and dielectric dispersion of spherical polyelectrolyte brushes *Langmuir* **28** 16372–81
- [23] Cametti C *et al* 2011 Dielectric relaxations of ionic thiol-coated noble metal nanoparticles in aqueous solutions: electrical characterization of the interface *Langmuir* **27** 7084–90
- [24] Chronopoulou L *et al* 2012 PLGA-based nanoparticles: effect of chitosan in the aggregate stabilization. A dielectric relaxation spectroscopy study *Colloids Surf. B* **97** 117–23
- [25] Guerrero-Martínez A, Pérez-Juste J and Liz-Marzán L M 2010 Recent progress on silica coating of nanoparticles and related nanomaterials *Adv. Mater.* **22** 1182–95
- [26] Ohshima H 1995 Electrophoresis of soft particles *Adv. Colloid Interface Sci.* **62** 189–235
- [27] Duval J F and Ohshima H 2006 Electrophoresis of diffuse soft particles *Langmuir* **22** 3533–46
- [28] Ohshima H 2008 Donnan potential and surface potential of a spherical soft particle in an electrolyte solution *J. Colloid Interface Sci.* **323** 92–7
- [29] Ohshima H 2012 Electrical phenomena in a suspension of soft particles *Soft Matter* **8** 3511–4
- [30] Schwan H *et al* 1962 On the low-frequency dielectric dispersion of colloidal particles in electrolyte solution *J. Phys. Chem.* **66** 2626–35
- [31] Delgado A *et al* 1998 The effect of the concentration of dispersed particles on the mechanisms of low-frequency dielectric dispersion (LFDD) in colloidal suspensions *Colloids Surf. A* **140** 139–49
- [32] O'Brien R 1986 The high-frequency dielectric dispersion of a colloid *J. Colloid Interface Sci.* **113** 81–93
- [33] Cametti C 2011 Dielectric properties of soft-particles in aqueous solutions *Soft Matter* **7** 5494–506
- [34] Wu H and Zhao K 2015 Dielectric relaxation of spherical polyelectrolyte brushes: movement of counterions and electrical properties of the brush layer *Langmuir* **31** 8566–76
- [35] López-García J, Grosse C and Horno J 2003 Numerical study of colloidal suspensions of soft spherical particles using the network method: 1. DC electrophoretic mobility *J. Colloid Interface Sci.* **265** 327–40
- [36] Hanai T, Asami K and Koizumi N 1979 Dielectric theory of concentrated suspensions of shell *Bull. Inst. Chem. Res. Kyoto Univ.* **57** 297–305
- [37] Asami K, Hanai T and Koizumi N 1980 Dielectric approach to suspensions of ellipsoidal particles covered with a shell in particular reference to biological cells *Japan. J. Appl. Phys.* **19** 359
- [38] Dukhin S S, Shilov V N and Bikerman J 1974 Dielectric phenomena and double layer in disperse systems and polyelectrolytes *J. Electrochem. Soc.* **121** 154C
- [39] Grosse C and Zimmerman V 2005 Numerical calculation of the dielectric and electrokinetic properties of vesicle suspensions *J. Phys. Chem. B* **109** 18088–95
- [40] Asami K 2014 Low-frequency dielectric dispersion of bacterial cell suspensions *Colloids Surf. B* **119** 1–5
- [41] Hanai T *et al* 1988 The number of interfaces and the associated dielectric relaxations in heterogeneous systems *Ferroelectrics* **86** 191–204
- [42] Jones T B 1995 *Electromechanics of Particles* (New York: Cambridge University Press)
- [43] Grosse C and Shilov V N 1996 Theory of the low-frequency electrorotation of polystyrene particles in electrolyte solution *J. Phys. Chem.* **100** 1771–8
- [44] Hanai T 1968 Electrical properties of emulsions *Emulsion Sci.* ed Ph Sherman (London: Academic) pp 354–477
- [45] O'Konski C T 1960 Electric properties of macromolecules. V. Theory of ionic polarization in polyelectrolytes *J. Phys. Chem.* **64** 605–19
- [46] Fouassier J-P 1995 *Photoinitiation, Photopolymerization, and Photocuring: Fundamentals and Applications* (Munich: Hanser)
- [47] Wang X *et al* 2011 Synthesis of spherical polyelectrolyte brushes by photoemulsion polymerization with different photoinitiators *Ind. Eng. Chem. Res.* **50** 3564–9
- [48] Schwan H 1963 Determination of biological impedances *Physical Techniques in Biological Research* ed W L Nastuk (New York: Academic)
- [49] Hanai T, Imakita T and Koizumi N 1982 Analysis of dielectric relaxations of w/o emulsions in the light of theories of interfacial polarization *Colloid Polym. Sci.* **260** 1029–34

- [50] Serghei A *et al* 2009 Electrode polarization and charge transport at solid interfaces *Phys. Rev. B* **80** 184301
- [51] Iacob C *et al* 2008 Charge transport and glassy dynamics in imidazole-based liquids *J. Chem. Phys.* **129** 234511
- [52] Mapesa E U *et al* 2014 Molecular dynamics of itraconazole confined in thin supported layers *RSC Adv.* **4** 28432–8
- [53] Allen R and Hansen J-P 2003 Electrostatic interactions of charges and dipoles near a polarizable membrane *Mol. Phys.* **101** 1575–85
- [54] Ballenegger V and Hansen J-P 2005 Dielectric permittivity profiles of confined polar fluids *J. Chem. Phys.* **122** 114711
- [55] Gawrisch K *et al* 1992 Membrane dipole potentials, hydration forces, and the ordering of water at membrane surfaces *Biophys. J.* **61** 1213
- [56] Saiz E *et al* 1981 Direction of the dipole moment in the ester group *J. Phys. Chem.* **85** 3211–5
- [57] Alvarez C *et al* 1997 Conformational and experimental studies on the dipole moments of models of comblike polymers *Macromolecules* **30** 6369–75
- [58] Gregory J *et al* 1997 The water dipole moment in water clusters *Science* **275** 814–7
- [59] Dominguez-Espinosa G *et al* 2008 Optical tweezers to measure the interaction between poly (acrylic acid) brushes *Polymer* **49** 4802–7
- [60] Groenewegen W *et al* 2000 Counterion distribution in the coronal layer of polyelectrolyte diblock copolymer micelles *Macromolecules* **33** 4080–6
- [61] Groenewegen W *et al* 2000 Neutron scattering estimates of the effect of charge on the micelle structure in aqueous polyelectrolyte diblock copolymer solutions *Macromolecules* **33** 3283–93
- [62] Van der Maarel J *et al* 2000 Salt-induced contraction of polyelectrolyte diblock copolymer micelles *Langmuir* **16** 7510–9
- [63] Russell J M 1988 Simple models for teaching equilibrium and Le Châtelier's principle *J. Chem. Educ.* **65** 871
- [64] Schneider C *et al* 2008 Microsurface potential measurements: repulsive forces between polyelectrolyte brushes in the presence of multivalent counterions *Langmuir* **24** 10612–5
- [65] Gambinossi F, Mylon S E and Ferri J K 2015 Aggregation kinetics and colloidal stability of functionalized nanoparticles *Adv. Colloid Interface Sci.* **222** 332–49
- [66] Butt H-J, Graf K and Kappl M 2006 *Physics and Chemistry of Interfaces* (New York: Wiley)
- [67] De Gennes P 1987 Polymers at an interface; a simplified view *Adv. Colloid Interface Sci.* **27** 189–209
- [68] Elmahdy M M *et al* 2009 Forces of interaction between poly (2-vinylpyridine) brushes as measured by optical tweezers *Macromolecules* **42** 9096–2